Atmospheric
Chemistry
and Physics
Discussions

Open Access

Peroxynitric acid (HO$_2$NO$_2$) measurements during the UBWOS 2013 and 2014 studies using iodide ion chemical ionization mass spectrometry

P. R. Veres[1,2], J. M. Roberts[2], R. J. Wild[1,2], P. M. Edwards[1,2,3], S. S. Brown[2], T. S. Bates[4,5], P. K. Quinn[5], J. E. Johnson[4], R. J. Zamora[6], and J. de Gouw[1,2]

[1]Cooperative Institute for Research in Environmental Sciences, University of Colorado, Boulder, Colorado, USA
[2]Chemical Sciences Division, NOAA Earth System Research Laboratory, Boulder, CO, USA
[3]Now at Department of Chemistry, University of York, York, YO10 5DD, UK
[4]Joint Institute for the Study of the Oceans and Atmosphere, University of Washington, Seattle, WA, USA
[5]NOAA PMEL, Seattle, WA, USA
[6]Physical Sciences Division, NOAA Earth System Research Laboratory, Boulder, CO, USA

Discussion Paper | Discussion Paper | Discussion Paper | Discussion Paper

ACPD

15, 3629–3666, 2015

Peroxynitric acid (HO$_2$NO$_2$) measurements during UBWOS 2013 and 2014

P. R. Veres et al.

Title Page

Abstract | Introduction

Conclusions | References

Tables | Figures

|◄ | ►|

◄ | ►

Back | Close

Full Screen / Esc

Printer-friendly Version

Interactive Discussion

Peroxynitric acid (HO$_2$NO$_2$) measurements during UBWOS 2013 and 2014

P. R. Veres et al.

Title Page

Abstract	Introduction
Conclusions	References
Tables	Figures

|◄ ►|

◄ ►

Back Close

Full Screen / Esc

Printer-friendly Version

Interactive Discussion

Abstract

Laboratory work is reported here establishing iodide ion chemical ionization mass spectrometry (I$^-$ CIMS) as a sensitive method for the unambiguous detection of peroxynitric acid (HO$_2$NO$_2$, PNA). A dynamic calibration source for HO$_2$NO$_2$, HO$_2$, and HONO was developed and calibrated using a novel total NO$_y$ detector (NO$_y$ CaRDS). Photochemical sources of these species were used for the calibration and validation of the I$^-$ CIMS instrument for detection of HO$_2$NO$_2$. A dual inlet system was developed to determine differences in the instrument response when using a heated inlet dissociator (150 °C) and a "cold" room-temperature inlet. HO$_2$NO$_2$ was detected as I-HO$_2^-$ (m/z 160), NO$_3^-$ (m/z 62) and I-HO$_2$NO$_2^-$ (m/z 206). The I$^-$ CIMS normalized sensitivity to peroxynitric acid was 2.0 Hz pptv^{-1} with a detection limit (3σ) of 40 pptv via detection of the I-HO$_2^-$ (m/z 160) cluster ion using an inlet dissociator at a temperature of 150 °C. Alternatively, PNA was detected via I$^-$ CIMS with a cold inlet at both the NO$_3^-$ (m/z 62) and I-HO$_2$NO$_2^-$ (m/z 206) ions with normalized detection sensitivities of 144 and 0.4 Hz pptv^{-1} respectively. The cold inlet sensitivity of iodide CIMS towards the detection of HO$_2$ radicals, also via detection at the I-HO$_2^-$ cluster ion, a potential HO$_2$NO$_2$ interference, was approximately 2.6 Hz pptv^{-1} with an instrumental detection limit (3σ) of 20 pptv. Ambient observations of HO$_2$NO$_2$ using I$^-$ CIMS were made during the 2013 and 2014 Uintah Basin Wintertime Ozone Study (UBWOS) are presented. Strong inversions leading to a build-up of many primary and secondary pollutants as well as low temperatures drove daytime HO$_2$NO$_2$ as high as 1.5 ppbv during the 2013 study. A comparison of HO$_2$NO$_2$ observations to mixing ratios predicted using a chemical box model describing an ozone formation event observed during the 2013 wintertime shows agreement in the daily maxima HO$_2$NO$_2$ mixing ratio, but a significant difference os several hours in the timing of the observed maxima. Observations of vertical gradients suggest that the ground snow surface potentially serves as both a net sink and source of HO$_2$NO$_2$ depending on time of day. Sensitivity tests using a chemical

box model indicate that the lifetime of HO_2NO_2 with respect to deposition has a non-negligible impact on ozone production rates on the order of 10 %.

1 Introduction

Hydrogen oxides ($HO_x = HO_2 + OH$) and nitrogen oxides ($NO_x = NO_2 + NO$) play central roles in atmospheric photochemistry. HO_2, a product of OH-initiated VOC oxidation, reacts with NO to produce NO_2, a key step in the photochemical ozone formation cycle in the troposphere. Peroxynitric acid (often referred to as PNA, HO_2NO_2, or HNO_4) plays an important role in the coupling of atmospheric HO_x and NO_x cycles (Niki et al., 1977), especially at low temperatures. PNA serves as an important HO_x and NO_x reservoir species altering the oxidative capacity of the atmosphere on regional and global scales (Kim et al., 2007; Chen et al., 2001; Davis et al., 2001; Carpenter et al., 2000).

PNA is formed via the reaction of HO_2 and NO_2 (DeMore et al., 1997; Sander et al., 2011).

$$HO_2 + NO_2 \xrightarrow{M} HO_2NO_2 \qquad (R1)$$

Formation via Reaction (R1) is favored at low temperatures and high pressures (Kim et al., 2007). Unimolecular decomposition is temperature dependent and occurs on a timescale of approximately 10 s at 1 atm, 298 K with the lifetime rapidly increasing to hours at 258 K (Gierczak et al., 2005);

$$HO_2NO_2 \xrightarrow{M} HO_2 + NO_2 \qquad (R2)$$

PNA can be lost via photolysis in the near ultraviolet (Jimenez et al., 2005) and near infrared via an overtone band (Roehl et al., 2002; Stark et al., 2008);

$$HO_2NO_2 \xrightarrow{\lambda} OH + NO_2 \qquad (R3)$$

$$HO_2NO_2 \xrightarrow{\lambda} HO_2 + NO_2 \qquad (R4)$$

Or by reaction with OH (Jimenez et al., 2004);

$$HO_2NO_2 + OH \longrightarrow H_2O + NO_2 + O_2 \tag{R5}$$

In the lower troposphere, Reactions (R3)–(R5) typically occur on timescales of days to months thereby implying that the dominant loss of PNA in the lower troposphere is typically unimolecular dissociation or deposition.

Deposition of PNA on snow surfaces has been observed in various studies where the atmospheric lifetime of PNA in Polar Regions is largely controlled by dry deposition (Huey et al., 2004; Slusher et al., 2002; Jones et al., 2014). Additional laboratory studies have been performed confirming the efficient uptake of PNA to ice (Li et al., 1996; Ulrich et al., 2012) and sulfuric acid solutions (Zhang et al., 1997). Dependent on the fate of PNA after deposition, the formation and subsequent deposition of PNA has been suggested to result in a net loss of HO_x and an increase in NO (Grannas et al., 2007), with Reactions (R1)–(R5) thereby having an impact on tropospheric ozone formation (Salawitch et al., 2002).

Observations of PNA are generally limited in scope with most measurements focusing on polar regions (Slusher et al., 2002, 2010; Huey et al., 2004), the free troposphere (Murphy et al., 2004; Singh et al., 2006, 2007; Keim et al., 2008; Kim et al., 2007), and the stratosphere (Rinsland et al., 1996, 1986; Sen et al., 1998). Mean PNA observations from these studies range from tens of pptv in polar surface regions to several hundred pptv in the upper troposphere/lower stratosphere. The impacts of PNA on upper tropospheric chemistry have been widely discussed (Brune et al., 1999; Wennberg et al., 1999; Faloona et al., 2000), with one study in particular identifying a PNA contribution as high as 20 % of the total NO_y budget (Murphy et al., 2004). Lower-tropospheric, mid-latitude measurements, in contrast, remain largely unexplored with the exception of, to our knowledge, a single airborne study conducted in Mexico (Spencer et al., 2009) where PNA concentrations up to 600 pptv were observed, and were correlated with O_3 formation.

The general lack of lower-tropospheric, mid-latitude observations is driven in part by two factors (i) a diminished atmospheric impact of PNA due to higher rates of thermal decomposition with respect to the generally colder polar and upper atmosphere, and (ii) a lack of instrumentation capable of providing sensitive unambiguous measurements

5 of PNA. Many of the techniques available measure PNA as a component of NO$_y$ using O$_3$/NO chemiluminescence (Keim et al., 2008) or total peroxynitrates via thermal decomposition laser induced fluorescence (Murphy et al., 2004). Currently available instrumentation capable of unambiguous measurement of PNA is limited to remote sensing detection via IR absorption spectroscopy (Rinsland et al., 1986, 1996; Sen

10 et al., 1998) or in-situ measurement via chemical ionization mass spectrometry using the SiF$_6^-$ ion (Slusher et al., 2002, 2001; Huey, 2007), or CF$_3$O$^-$ (Spencer et al., 2009; Huey et al., 1996). Among these, CIMS techniques have been shown to have sufficient sensitivity and time resolution for the in-situ monitoring of PNA concentrations in the lower troposphere.

15 In this work, we present laboratory and ambient measurements illustrating the utility of iodide ion CIMS for unambiguous measurement of PNA. Additionally, we show applicability of this technique for the detection of both HO$_2$ and HONO, atmospheric species that are also integral to HO$_x$ and NO$_x$ cycles. These results were necessary in order to rule out potential mass overlap or PNA interferences from the sampling of HO$_2$

20 and HONO. A photo-source has been developed for dynamic production of PNA, HO$_2$, and HONO to assist with laboratory calibration and elucidation of various ionization schemes. PNA observations made during the 2013 and 2014 Uintah Basin Wintertime Ozone Study (UBWOS) will be presented and compared to a chemically explicit box model developed to describe the air quality in the Uintah basing during a high ozone

25 event observed during the 2013 study (Edwards et al., 2014). The impact of PNA on HO$_x$ and NO$_x$ budgets, particularly as it relates to the photochemical production of ozone, will also be discussed.

2 Experimental setup

We present both laboratory and field data collected over a two-year period encompassing the 2013 and 2014 UBWOS field studies. The following describes the instrumentation used in this work as well as a short description of the UBWOS study and field conditions. Information and links pertaining to the 2013 and 2014 Uintah Basin Winter Ozone Studies are available on the web (http://esrl.noaa.gov/csd/groups/csd7/measurements/2013ubwos/).

2.1 Instrumentation

2.1.1 Iodide ion CIMS (I⁻ CIMS)

The I$^-$ CIMS instrument consists of an ion flow tube coupled to a quadrupole mass spectrometer. Briefly, CH_3I in N_2 is passed through a ^{210}Po ionizer resulting in the production of iodide (I$^-$) ions. Subsequently, I$^-$ reacts in the flow tube with a sample gas resulting in the production of anions that are mass filtered using a quadrupole mass spectrometer and detected. Additional details about the instrument can be found elsewhere (Slusher et al., 2004). The instrumental differences with respect to that described in Slusher et al. (2004) will be discussed as they relate to the field deployments and laboratory measurements presented.

The sensitivity of the I$^-$ CIMS to the species presented in this work (HO_2NO_2, HONO, and HO_2) is dependent on the degree of water clustering present in the flow tube. Some ionization reactions occur faster through the I-H_2O^- cluster, likely as a result of ligand switching via an intermediate cluster ion, while other reactions are independent of the water cluster population. Even with a declustering region present, the ratio of the first water cluster to the parent ion is a valuable diagnostic and can often be a more appropriate way to account for changes in the primary ion signal through normalization of measured signals to the sum of I$^-$ and I-H_2O^-, as was performed in this work.

The extent of the ion clustering in the I$^-$ CIMS can be controlled using a collisional dissociation chamber and through addition of water directly into the flow tube to modify the expected ionization chemistry. In this study, the ratio of the iodide water cluster ion (I-H$_2$O$^-$, m/z 145) to the iodide ion (I$^-$, m/z 127) ranged from approximately 5 % to 50 % and was adjusted to maximize the instrument sensitivity towards individual species or classes of compounds depending on the application. I$^-$ CIMS was operated in the laboratory with a switchable inlet to allow for sampling through a section of PFA tubing (0.025 m) either at room temperature ("cold") or operated as an inlet dissociator (130 °C, "hot").

The inlet configuration used during the 2014 UBWOS study was identical to that used in the laboratory experiments, where inlet switching could be performed to sample from either a "cold" or "hot" inlet. During the 2013 UBWOS study, however, the I$^-$ CIMS did not employ a switchable inlet; rather a "hot" inlet dissociator at 150 °C was used throughout the entire measurement period. Never-the-less post experiment tests with the inlet configuration used during UBWOS 2013 permit us to quantify HO$_2$NO$_2$ during that study, albeit with increased uncertainty.

2.1.2 Total NO$_y$ cavity ring down instrument

During the laboratory portion of this work a novel, four channel laser diode based cavity ring-down (CRD) instrument was used to quantify NO, NO$_2$ and NO$_y$. Details of the NO$_y$ CRD instrumentation can be found elsewhere (Wild et al., 2014). Briefly, NO$_y$ is thermally dissociated to NO and NO$_2$ in a heated quartz inlet. Any NO in the sample air or formed via catalysis is converted to NO$_2$ by addition of O$_3$ after the quartz converter. Quantification of NO$_2$ in the sample is performed using cavity ring-down at 405 nm.

The quartz converter is typically operated with a gas temperature of 720 °C, however, the temperature can be adjusted downward to measure specific classes of compounds or individual species that contribute to total NO$_y$ while excluding unwanted interferences. A similar method has been used previously for the speciation of NO$_y$ in both ambient and field measurements (Wooldridge et al., 2010; Day et al., 2002). In these

experiments, the gas temperature in the converter was optimized for detection of PNA and HONO, 130 and 720 °C respectively, a set point determined by scanning the quartz heater through the entire temperature range as shown in Wild et al., 2014 (Wild et al., 2014). A detailed discussion on the application of this technique towards the quan-
5 tification of HONO and PNA generated in a dynamic laboratory calibration source is included below.

2.2 Field site description

An I$^-$ CIMS instrument was deployed during the 2013 and 2014 UBWOS field studies conducted in the Uintah basin, UT. The goal of these studies was to improve our under-
10 standing of the chemistry leading to wintertime observations of elevated ozone levels within the basin. The field site configuration in 2014 is best described by the UBWOS 2012 field report (Lyman and Shorthill, 2012) where a nearly identical site design was employed while a detailed description of the 2013 measurements is available in the UBWOS 2013 field report (Stoeckenius and McNally, 2014).
15 During both the 2013 and 2014 studies, observations of HO_2NO_2 gradients over snow were conducted by using a moveable (7 m, 35 °C) PFA inlet during the 2013 study and a switchable dual inlet system (each inlet was 20 m, 30 °C) for the 2014 study. The total inlet flow used during the 2014 study was approximately 20 slpm from which the I$^-$ CIMS subsampled 2 slpm. During the 2013 study, a total inlet flow of 2 slpm was
20 sampled through a short stainless steel section attached to the end of a PFA inlet and heated to a temperature of 65 °C, to dissociate N_2O_5 prior to sampling preventing $ClNO_2$ interferences due to reactions on the inlet surface (Behnke et al., 1997). In this inlet, HO_2NO_2 will dissociate as well as recombine, considering the stability of HO_2 on PFA surfaces. The CIMS instrument in 2013 was not configured to monitor the I-HO_2^- or
25 I-$HO_2NO_2^-$ ions, however, NO_3^-, routinely monitored for diagnostic purposes, provides a means to estimate ambient HO_2NO_2 as a result of the large sensitivity of the CIMS to HO_2NO_2 at this ion.

In addition to gas phase measurements conducted at the field site, snow samples were collected daily throughout the UBWOS 2013 study. Surface samples were collected from the top 3 cm of snow from undisturbed locations within 1.3 km of the field site. At each site, 2 to 6 1 L glass jars were collected and kept frozen until analysis, typically within 48 h of sampling. Prior to analysis via an ion chromatograph (IC), samples were melted and filtered using a 25 mm diameter 0.4 µm pore size nucleopore filter. Filtered samples were subsequently injected directly into the IC and analyzed for anions (e.g. Cl^-, NO_2^-, NO_3^-) and cations (e.g. Na^+, NH_4^+, K^+).

3 Results and discussion

Laboratory experiments using I^- CIMS were preformed both in preparation and upon the conclusion of the UBWOS 2014 study. The goal of these experiments was to adapt the I^- CIMS technique for the sensitive detection of PNA and develop a method for calibration. The development of an HO_2 based photolysis source for the production of HO_2NO_2 also led to the recognition that the I^- CIMS can be applied to the direct measurement of HO_2 radicals. Additionally, the HO_2 photolysis source is readily adaptable for the production of an on-line HONO calibration standard. These laboratory developments in calibration standard production and I^- CIMS detection of PNA, HONO, and HO_2 will be discussed in detail in the following sections. Lastly, PNA observations from the 2013 and 2014 UBWOS study will be presented along with a discussion of the results with respect to a chemically explicit box model developed to describe observations from the 2013 UBWOS study (Edwards et al., 2014).

3.1 Standard generation and detection

The following describes the ion molecule reactions with I^- ions resulting in the detection of HO_2NO_2, $HONO$ and HO_2:

$$I^- + HO_2 \longrightarrow I \bullet HO_2^- \tag{R6}$$

$$I^- + HO_2NO_2 \longrightarrow I \bullet HO_2NO_2^- \tag{R7}$$

$$I^- + HO_2NO_2 \longrightarrow HOI + NO_3^- \tag{R8}$$

$$HO_2NO_2 \xrightarrow{\Delta} HO_2 + NO_2 \xrightarrow{I^-} I \bullet HO_2^- \tag{R9}$$

$$I^- + HONO \longrightarrow I \bullet HONO^- \tag{R10}$$

where Reaction (R7) is only observed using a "cold" inlet while Reaction (R9) occurs upon thermal dissociation of PNA in the inlet. Experimentally, the above reactions, with the exception of Reaction (R8), were observed in this work to occur predominantly via reaction of the hydrated iodide cluster (I-H_2O^-, m/z 145) based on the strong dependence of sensitivity on water vapor observed during these experiments. This implies that the above reactions are ligand switching reactions made faster by the ability of H_2O to accommodate excess energy of reaction through extra degrees of freedom up to and including dissociation.

Normalized (10^6 cps I^-), background corrected mass spectra are shown in Fig. 1 for each of the sources. The ratio of m/z 145 (I-H_2O^-) to m/z 127 (I^-) is displayed as a percentage on each panel for reference. These spectra represent the result of the subtraction of a normalized background mass spectrum from a sample spectrum. The background that was applied varies for each species and is dependent on the sample matrix, which will be described separately in the following sections. In all cases, the mass ranges from 126 to 128 and 144 to 146 corresponding to the I^- (m/z 127) and I-H_2O^- (m/z 145 ions were removed to simplify interpretation of the mass spectra. These spectra allow for the identification of impurities in the photolysis sources used

as well as demonstrating the ions that were used for the unambiguous detection of each analyte. Each of these sources will be discussed in detail in the following sections.

3.1.1 HO$_2$ radical

HO$_2$ radicals are generated in the laboratory via photolysis of H$_2$O in the presence of O$_2$ (Dusanter et al., 2008). A mixture of approximately 100 sccm N$_2$ and 0.5 sccm O$_2$ was bubbled through water and diluted into a 5 slpm flow of N$_2$. The mixture is subsequently passed into a PFA photolysis cell and irradiated with a 185 nm Pen-Ray$^{®}$ lamp. The N$_2$ dilution flow is produced using boil off from a high-pressure liquid nitrogen Dewar to limit the amount of NO$_x$ and VOC in the system. Detection of HO$_2$ via I$^-$ CIMS occurs through direct observation of the parent ion cluster (I-HO$_2$), therefore, it is not necessary to add CO in order to titrate OH as no measurement interference is expected. Addition of trace amounts of CO will increase the concentration of HO$_2$ produced, though trace amounts of NO and NO$_2$ from the steel cylinder mixture result in an increase in PNA and HONO backgrounds with increasing CO.

Figure 1a shows the difference mass spectrum of the HO$_2$ radical mixture less the instrument background. In this case, the instrument background was the ion signal measured prior to turning on the 185 nm lamp. It is clear from the mass spectrum that there is only a single dominant peak observed at m/z 160 (I-HO$_2^-$). A method for the quantitative calibration of the HO$_2$ radical source and the I$^-$ CIMS instrument for the detection of HO$_2$ radicals will be discussed in Sect. 3.1.4. The sensitivity of I$^-$ CIMS to the detection of HO$_2$ was determined to be a function of the mixing ratio of water in the flow tube as well as the extent of clustering/declustering in the system, e.g. reduction of the I-H$_2$O$^-$: I$^-$ ratio due to higher E/N in the declustering region, results in a lower observed sensitivity. Additional work to characterize the effect of humidity on the detection efficiency is necessary to refine the potential of this method for ambient monitoring of HO$_2$.

The difficulty of quantitative sampling through an inlet is a significant limitation to the measurement of radicals in the atmosphere. Laboratory experiments were performed to probe the effect of inlet length on sampling of HO_2 radicals produced in N_2. The results are shown in Fig. 2a, as the count rate at a given residence time normalized to the count rate at the shortest residence time. This reaction is likely first order in HO_2 therefore a log-linear fit is the most appropriate representation of the data, however the data has been fit using a linear curve for simplicity. HO_2 is lost at a rate of approximately $0.60\,s^{-1}$ in a 6 mm o.d. PFA inlet. Results indicate that the loss of HO_2 is driven not by surface losses, but loss of HO_2 via reaction with residual NO_2 in the system to produce HO_2NO_2, as can be observed in the nearly equivalent rate of increase in observed HO_2NO_2 ($0.67\,s^{-1}$, Fig. 2b). Qualitative observations of H_2O_2, at m/z 161 ($I\text{-}H_2O_2^-$), during the same experiment suggest that there is no loss of HO_2 via self-reaction occurring on these timescales.

3.1.2 Peroxy nitric acid (HO$_2$NO$_2$, PNA)

Two methods were used in this work for the production of a PNA standard. In the first of these methods, PNA was synthesized using the techniques described in Appelman and Gosztola (1995). Briefly, a nitrite-peroxide solution ($NaNO_2$ in 30 % H_2O_2) is mixed with a peroxide-acid solution (30 % H_2O_2 in 70 % $HClO_4$) at $-20\,°C$ to produce approximately 1.7 M PNA in H_2O_2. The resulting solution is placed in a glass diffusion cell, (Williams et al., 2000), at a temperature of $-20\,°C$ with zero air passed over the headspace to produce a dynamic mixture of PNA. The 20 sccm diffusion source outflow was sampled directly into the inlet flow of the I^- CIMS. This method of synthesis also results in the production of non-negligible amounts of HNO_3 and H_2O_2. While nylon wool can be used to semi-selectively remove HNO_3 from the calibration flow, no method for the selective removal of H_2O_2 was identified. In any case, HNO_3 and H_2O_2 are observed at unique m/z ions and therefore do not interfere with PNA measurement.

Alternatively, PNA can be dynamically generated using the output of the HO$_2$ source described in Sect. 2.2.1 (Ulrich et al., 2012). Addition of NO$_2$ to the output of the HO$_2$ radical source results in the production of PNA. Due to the relative simplicity of this technique, photo-production of PNA was used as the preferred I$^-$ CIMS calibration method for the laboratory and field measurements.

Figure 1 shows a difference mass spectrum of HO$_2$NO$_2$ detected using an iodide CIMS instrument with a "cold" inlet (Fig. 1b) and an inlet dissociator temperature of 130 °C (Fig. 1c). In both cases, the instrument background was chosen as the ion signal prior to the addition of NO$_2$. When using a "cold" inlet, $\sim$ 30 °C, the dominant peak observed is m/z 62 (NO$_3^-$), Reaction (R8). An ion signal at m/z 206 (I-HO$_2$NO$_2^-$) is also observed, although to a much lesser extent than m/z 62 (NO$_3^-$), An ion signal at m/z 206 (I-HO$_2$NO$_2^-$), Reaction (R7), is also observed, although to a much lesser extent than m/z 62 (NO$_3^-$). When an inlet dissociator is used, HO$_2$NO$_2$ is observed at m/z 62 (NO$_3^-$) and m/z 160 (I-HO$_2^-$), where the detection of PNA at m/z 62 (NO$_3^-$) results from incomplete thermal dissociation of HO$_2$NO$_2$ in the inlet.

3.1.3 HONO

Similarly to PNA, HONO can be formed by addition of NO to the output of the HO$_2$ source described in Sect. 3.1.1. Addition of excess NO to the HO$_2$ calibration source results in the production of HONO from titration of HO$_2$, as well as any OH produced in the source, via the following reactions:

$$HO_2 + NO \longrightarrow OH + NO_2 \tag{R11}$$
$$OH + NO \longrightarrow HONO \tag{R12}$$

Figure 1d shows the difference mass spectrum of the HONO calibration source, where the instrument background here was chosen as the ion signal prior to the addition of NO. It is clear from the figure that HONO is the only product formed and is detected by I$^-$ CIMS at m/z 174 (I-HONO$^-$).

This method of HONO production is instantaneous and does not require the period of stabilization that is necessary for acid-salt reaction based sources (Febo et al., 1995). HONO standard production via the reaction of HO_2 and NO provides a good alternative to previously used I^- CIMS calibration methods (Roberts et al., 2010).

3.1.4 Dynamic source calibration

Quantification of PNA and HONO produced using the above-described methods was performed using a novel quartz catalysis total NO_y instrument (Wild et al., 2014), described in Sect. 2.2.2. Laboratory experiments indicate that more than 99 % of PNA is thermally dissociated above a temperature of 100 °C while HONO decomposition is negligible below 200 °C. The quartz inlet was operated at gas temperatures of 160 °C and 720 °C for the measurement of PNA and HONO, respectively. The difference in total NO_y minus the sum of NO_2 detected yields a quantitative measurement of the PNA or HONO produced in the source.

During these experiments the calibration source flow was alternately sampled by the I^- CIMS and CRD instruments. In order to eliminate any differences in radical reaction times, as a result of inconsistencies in the inlet lengths between the two instruments, the gaseous mixture was passed over glass wool subsequent to addition of NO or NO_2 to terminate the reaction by removing any remaining HO_2 radicals. In this manner the I^- CIMS sensitivity is calculated as the ratio of the I^- CIMS ion signal to the CaRDS measured concentrations. A summary of instrument sensitivities and detections limits (3σ) is included in Table 1. For the calibration data reported in Table 1, the m/z 145 to m/z 127 ratio was approximately 30 %.

The I^- CIMS sensitivity towards HONO at the I-HONO$^-$ cluster (m/z 174), Reaction (R10), was determined to be 1.7 Hz ppbv^{-1} with a corresponding 3σ instrumental detection limit of 30 pptv. The detection limit for HONO is largely limited by the magnitude of the ever-present I-NO$_2^-$ (m/z 173) ion and the low resolution of the quadrupole mass spectrometer used in this work. The HONO sensitivity reported here represents

detection with a 25 °C inlet, however, the instrument sensitivity was found to be nearly equivalent, within the stated uncertainties, using the heated (130 °C) dissociator.

The sensitivity towards PNA was determined for detection at the I-HO$_2$NO$_2^-$ (m/z 206, 25 °C inlet), I-HO$_2^-$ (m/z 160, 130 °C inlet), and NO$_3^-$ (m/z 62, 25 °C inlet) ions, Reactions (R7) though (R9) respectively. The most sensitive method of detection was observed via NO$_3^-$ in a 25 °C inlet, 144 Hz pptv^{-1} with a corresponding 3σ detection limit of 0.7 pptv. Detection at the I-HO$_2^-$ and I-HO$_2$NO$_2^-$ ions are considerably less sensitive, 2.0 and 0.4 Hz pptv^{-1} respectively. The 3σ detection limits are approximately 40 and 20 pptv for I-HO$_2^-$ and I-HO$_2$NO$_2^-$ respectively.

While the most sensitive detection of PNA occurs via NO$_3^-$, there exist several potential interferences that are also observed at that ion, see Table 1 in Wang et al., 2014 (Wang et al., 2014). Considering the sensitivity to PNA detection, relatively low daytime levels of PNA will result in significant signals at m/z 62. In fact, a recent study has suggested that evidence exists for a large daytime source of N$_2$O$_5$ detected via NO$_3^-$ ion using I$^-$ CIMS measurements (Wang et al., 2014); however, low daytime levels of HO$_2$NO$_2$ would also be consistent with observations presented in that work. Unfortunately, detection of PNA at m/z 160 (I-HO$_2^-$) leads to overlap with HO$_2$ radical detection at that mass. Therefore, we suggest that m/z 206 (I-HO$_2$NO$_2^-$) will yield the most reliable, interference free method of PNA detection for ambient measurements. Increasing the I-H$_2$O cluster ratio beyond 30 % (this study) should improve the instrument sensitivity towards detection of PNA at the m/z 206 cluster ion.

An indirect calibration was performed for the quantification of the HO$_2$ source, as no direct HO$_2$ measurement was readily available. An initial amount of HO$_2$ radicals are generated and monitored via the I$^-$ CIMS operated with a 25 °C inlet. A small amount of NO$_2$ is then added generating PNA with a corresponding reduction in observed I$^-$ CIMS HO$_2$ signal. The concentration of HO$_2$ lost by titration is assumed to be equivalent to the amount of PNA produced in the reaction, as the formation of PNA involves the consumption of one HO$_2$ radical per molecule. Using the previously described PNA

calibration method, the sensitivity can be calculated as the ratio of the reduction in the observed I^- CIMS $I-HO_2^-$ signal to the NO_y measured PNA concentration. The I^- CIMS detection sensitivity was determined using this method to be $2.6\,Hz\,pptv^{-1}$ with a corresponding 3σ detection limit of $20\,pptv$. As it was not the focus of this work, the instrument inlet was not optimized for the sampling of radical species; therefore changes in the inlet design and increases in the iodide-water cluster concentration in the flow tube would both serve to increase the instrument sensitivity and improve instrument detection limits to levels more appropriate for ambient sampling of HO_2.

3.2 Uintah Basin Wintertime Ozone Study (UBWOS) observations

Observations of HO_2NO_2 during the UBWOS 2014 study are shown in Fig. 3 for the entire duration of the measurement period. Measurements of the $I-HO_2NO_2^-$ ion using a cold inlet were performed only during the initial and final portion of the study for thirty minutes every hour. Ambient air was sampled through a heated inlet dissociator on alternating 30 min periods with "cold" sampling performed on the opposite time periods during the following: 24–30 January and 4–14 February. For the remainder of the measurements, 30 January–4 February, ambient air was continuously sampled through a heated dissociator. During sampling periods where the inlet dissociator was used PNA was monitored on m/z 160 ($I-HO_2$), and during periods of "cold" sampling via m/z 206 ($I-HO_2NO_2$). It is clear from the correlation plot inset in Fig. 3 that both sampling methods ("cold" and hot) agree reasonably well, slope = 0.93, $R^2 = 0.785$. There does appear to be a positive bias in the m/z 160 observations relative to detection at m/z 206, indicated by a positive intercept and clear disagreement during certain periods shown in the Fig. 3 timeseries. One possible explanation is the sensitivity at m/z 160 to ambient HO_2 or HO_2 generated in the inlet as a product of PNA decomposition. Given the length, temperature, and residence time of the inlet used (20 m, 30 °C, $\sim 4.8\,s$), PNA is expected to decompose by approximately 5 % prior to sampling. The HO_2 radicals produced as a result of PNA decomposition would likely be detected

via m/z 160 yet remain unobserved on the m/z 206 ion leading to a positive bias in m/z 160 observations. Additionally from laboratory results presented in Fig. 2b, we expect there to be production of HO_2NO_2 in the inlet; however, model approximations of the HO_2 mixing ratio during the 2013 study (15 pptv maximum) yields a maximum formation of HO_2NO_2 in the inlet during peak ozone events of ~ 1 % (Edwards et al., 2014).

Aside from the sampling conditions already described, several days of PNA measurements were performed during the 2014 study comparing a short unheated PFA inlet (3 m, ambient temperature) and a longer heated inlet (20 m, 30 °C). An average reduction of 5 % is observed in the PNA mixing ratio when sampling through the longer heated inlet as a result of thermal and perhaps surface assisted decomposition. It is important to note that the data presented here are not corrected for these inlet losses and are therefore considered a lower limit on ambient PNA.

During UBWOS 2013, the I^- CIMS was equipped to monitor PAN compounds using a thermal dissociation inlet, 150 °C. This was done prior to the laboratory work described in this manuscript and neither m/z 160 nor m/z 206 were monitored during the measurement period. However, the NO_3^- ion (m/z 62) was monitored throughout the entire campaign with observed signals exceeding 2e5 counts per second at times. Using the calibration data obtained from the laboratory portion of this work, an approximate PNA concentration was determined for the 2013 UBWOS study, assuming the same NO_3^- (m/z 62) sensitivity as measured during the laboratory calibrations performed after the 2014 study (144 Hz pptv^{-1}), corrected for differences in dissociator temperatures and transmission of HO_2NO_2 through the heated inlet tip used during the 2013 study. The error associated with this method was calculated to be approximately 60 %, largely due to corrections applied to account for differences in instrument tuning and additional HO_2NO_2 losses due to the different inlet conditions used during the two years.

Figure 4a shows the diurnal average of 2013 I^- CIMS observations of PNA for the entire study. Similarly to the 2014 measurements, also included in Fig. 4a, PNA reaches

Title Page

Abstract | Introduction

Conclusions | References

Tables | Figures

|◄ | ►|

◄ | ►

Back | Close

Full Screen / Esc

Printer-friendly Version

Interactive Discussion

a peak after solar maximum ($\sim$ 15:00 MST) with a minimum observed throughout the night. As such, N_2O_5, a nighttime species and potential interference on the NO_3^- ion, does not contribute to the observed daytime signal.

The PNA mixing ratios observed during the 2013 and 2014 studies are expected for cold conditions with active photochemistry and sufficient NO_x pollution. Displayed in Fig. 5 are the conditions necessary to sustain an equilibrium concentration of 1 ppbv PNA with respect to temperature and the mixing ratios of HO_2 and NO_2. The dashed area superimposed on the figure represents the approximate range of conditions encountered during the 2013 study, where HO_2 levels were approximated using model results that describe an ozone event observed during the 2013 study, described below. While the average diurnal mixing ratio peaks at 0.5 ppbv, mixing ratios up to 1.5 ppbv were observed during the 2013 study and can be explained by the coincidence of high daytime levels of NO_2 with the low temperatures in the Uintah basin.

As described previously, the vertical gradient of various species was probed through the use of a dual inlet system (30 and 1 m heights) during the UBWOS 2014 study. A comparison of those measurements for PNA is shown in Fig. 4a as diurnal averages of the measurements where dual inlet switching was applied. Figure 4b shows the result of the difference of the 1 m minus the 30 m PNA measurements. Displayed in this fashion, a positive value is an indication that PNA is larger in the surface coupled layer than aloft with the opposite indicating a relative enhancement of PNA in the layer decoupled from the surface. One interpretation of these results is that there is deposition of PNA to the snow surface throughout the night with a small emission from the snow surface in the early morning to midday. A similar result has been reported by Jones et al., 2014 (Jones et al., 2014), where evidence for surface exchange was observed for HO_2NO_2 and HNO_3 during the Antarctic winter. Unfortunately, fluxes of PNA were not measured directly in this study so further validation of this interpretation of the data is not possible. In any case, the dynamics causing these differences in PNA observations, whether mixing or deposition in origin, have a measureable impact on the ozone formation potential in the Uintah basin as will be discussed below.

Peroxynitric acid (HO₂NO₂) measurements during UBWOS 2013 and 2014

P. R. Veres et al.

Title Page

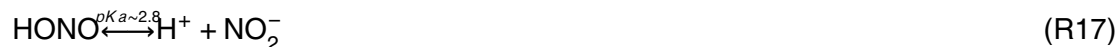| Abstract | Introduction |
| Conclusions | References |
| Tables | Figures |

Back | Close

Full Screen / Esc

Printer-friendly Version

Interactive Discussion

A chemical box model, based on the MCM v3.2 chemistry scheme, has been developed to describe observed ozone production during a wintertime ozone pollution episode during UBWOS 2013 (Edwards et al., 2014). This 0-D model contains a near-explicit oxidation mechanism for 32 observed VOC and oxidized VOC, and is constrained using constant emissions of primary species (VOC and NO), with the concentrations of all other species calculated by the chemistry scheme. Physical loss processes, such as mixing and deposition, are represented via a bimodal 1st order loss process for all species, the rate of which has been optimized based on boundary layer height observations and the concentrations of long lived species, e.g. methane.

Figure 6a and b display the base model calculation of PNA and ozone reported in the Edwards et al. (2014) study. While there is reasonable quantitative agreement between the model and measurement daily maxima, there is a temporal shift in PNA measurements relative to model predictions. While the reasons for this are as of yet unknown, possible explanations include underestimation in modeled NO, additional daytime PNA loss mechanisms, or issues with the simple parameterization of mixing used in the model. The latter seems unlikely as the model reproduces the observed diurnal variation in ozone relatively well. As discussed above, there is also evidence that PNA is lost to the snow surface, though the temporal trend in deposition implied from the gradient measurements does not suggest a relatively higher rate in the morning to early afternoon than in the evening, rather there is a possible indication of a mid-day snow surface source. Nitrogen oxides within the model are parameterized using a constant source of NO, with the partitioning of all nitrogen oxides calculated by the chemistry scheme. A quantitative comparison of NO observations to modeled values suggests that the model does typically underestimate the NO concentration throughout the morning. This underestimation would lead to an underestimation of the loss of HO_2 via reaction with NO, thereby slowing the formation rate leading to an over-prediction of PNA. This process would have a particular impact in the morning hours where observed NO is relatively large and HO_2 is limited.

Deposition of PNA has the potential to result in a net loss of HO_x and thus an increase in NO (Grannas et al., 2007), due to reduced titration to NO_2, which would have an overall effect on ozone formation potential. The sensitivity of ozone production in the UBWOS 2013 box model to changes in the lifetime of PNA with respect to deposition (t_{PNA}) was investigated and the results of these tests are displayed in Fig. 6. In addition to the 1st order physical loss term applied to all species, predominantly representing losses due to mixing (Edwards et al., 2014), an additional 1st order loss term for PNA was added to the model scheme to represent deposition. Calculations with a lifetime for PNA with respect to deposition (t_{PNA}) of 1 h yields approximately a 12 % reduction in daily max ozone from the base case where no PNA deposition was included. It is not possible using data from the UBWOS 2013 or 2014 study to determine the observed lifetime of PNA with respect to deposition to the snow surface; however the measurements and model suggest that surface deposition is occurring with a potentially measureable effect on the ozone production in the Uintah basin.

The post-depositional fate of PNA is also important as this scenario assumes that the loss of PNA to the snow surface is irreversible and thus a net HO_x and NO_x sink. Subsequent snow chemistry resulting in storage and volatilization of HO_x (Jones et al., 2014) or NO_x has the potential to reduce the magnitude of the effects observed in Fig. 6b. Subsequent to deposition and solvation in an aqueous solution, such as the snow surface in the Uintah basin, PNA can undergo the following dissociation and ionic reactions (Logager and Sehested, 1993; Zhu et al., 1993):

$$HO_2NO_{2(g)} \longleftrightarrow HO_2NO_{2(s)} \tag{R13}$$

$$HO_2NO_2 \overset{pKa\sim6}{\longleftrightarrow} H^+ + O_2NO_2^- \tag{R14}$$

$$HO_2NO_{2(s)} \longrightarrow HONO \tag{R15}$$

$$O_2NO_2^- \longrightarrow NO_2^- + O_2 \tag{R16}$$

$$HONO \overset{pKa\sim2.8}{\longleftrightarrow} H^+ + NO_2^- \tag{R17}$$

Previous work has shown that uptake of PNA to highly acidic surfaces results in reversible uptake, where chemical loss to NO_2^- is negligible (Zhang et al., 1997).

Measurements of snow surface nitrite made during the 2013 and 2014 study are shown in Fig. 7a and b, respectively, along with observations of PNA. Two pollution events observed in 2013 were separated by a cleanout event where additional precipitation (indicated by the blue shaded region in Fig. 7a) accompanied by higher winds and unstable conditions ventilated the basin. The nitrite content of the snow surface generally increases throughout the first event at a rate proportional to the daily increase in PNA mixing ratio until fresh snow is added and nitrite levels drop. Throughout the second event, nitrite levels in the snow surface again build up as ambient PNA levels also increase. We note here that any HO_2NO_2 dissolved in the snow can form NO_2^- with efficiencies as high as 56 % depending on pH (Goldstein et al., 2005).

A more detailed look at snow nitrite content shows a generally observed decrease in surface layer concentrations throughout the day, Fig. 7c, a result that is consistent with reversible uptake of nitrite. This daytime depletion of snow nitrite could be evidence of the reversible uptake of PNA, shown in Fig. 4a, or an indication of the formation and subsequent release of other nitrogen containing species, such as HONO, from the snow surface. It is interesting to note that the highest measurements of snow nitrite in a given day typically occur prior to the build up of ambient PNA. This result is consistent with nocturnal uptake of PNA or HONO to the snow surface, as shown in Fig. 4b; however, no evidence of this nighttime enrichment is available, as nighttime measurements of snow surface nitrite were not made. Additionally, the extent to which Reactions (R14) and (R16) were occurring, and therefore PNA contributing to snow nitrite content, cannot be approximated as the pH of the snow surface was not measured during this study.

Improved measurements of the deposition velocity on snow surfaces of varying acidities and the chemical fate of PNA after deposition is necessary to improve our understanding of the impacts of PNA deposition to HO_x and NO_x budgets. The post depositional fate of PNA can have a non-negligible impact on ozone formation potential,

particularly in cold regions, such as the Uintah basin, where the lifetime of PNA is sufficiently long such that deposition becomes a dominant sink. Considering the similar surface chemistry and influence on radical budgets for atmospheric HONO (Vanden-Boer et al., 2015), simultaneous measurement must be performed to understand the tropospheric fate of PNA and HONO species in cold regions and the extend of their involvement in tropospheric HO$_x$ and NO$_x$ budgets.

4 Conclusions

Laboratory studies have been conducted to demonstrate the utility of I$^-$ CIMS as a method for the quantitative detection of HO$_2$, PNA, and HONO. Methods for the production and calibration of on-line laboratory standards for HO$_2$, PNA, and HONO have been developed and described above. The I$^-$ CIMS technique offers an unambiguous method with sufficient sensitivity for the detection of PNA in mid latitude tropospheric regions, an area with a general lack of direct observations. Additionally, while it is not fully explored here, the application of I$^-$ CIMS for the direct detection of HO$_2$ has significant potential for use in future laboratory, chamber, and ambient measurements.

The I$^-$ CIMS instrument was deployed during the 2013 and 2014 UBWOS studies in the Uintah basin, UT during several wintertime ozone events. Field-based experiments illustrate that as a result of the thermal instability of PNA and the potential for formation within inlets, care must be taken to both characterize sampling inlets and minimize residence times in order to perform accurate quantitative measurements. PNA vertical gradient as well as correlation with snow surface nitrite content suggests that deposition, dissociation and ionic reactions of PNA could serve as a large surface nitrite source in the Uintah basin.

Comparison of the 2013 PNA observations to a chemically explicit box model yields quantitative agreement of daily maximum mixing ratios, but with disagreement in the diurnal cycle in late afternoon. Results of this comparison suggest that increased PNA deposition rates lead to an overall decrease in the ozone production potential in the

Title Page

Abstract | Introduction

Conclusions | References

Tables | Figures

|◄ | ►|

◄ | ►

Back | Close

Full Screen / Esc

Printer-friendly Version

Interactive Discussion

References

Appelman, E. H. and Gosztola, D. J.: Aqueous peroxynitric acid (HOONO$_2$): a novel synthesis and some chemical and spectroscopic properties, Inorg. Chem., 34, 787–791, 1995.

Behnke, W., George, C., Scheer, V., and Zetzsch, C.: Production and decay of ClNO$_2$, from the reaction of gaseous N$_2$O$_5$ with NaCl solution: bulk and aerosol experiments, J. Geophys. Res.-Atmos., 102, 3795–3804, doi:10.1029/96jd03057, 1997.

Brune, W. H., Tan, D., Faloona, I. F., Jaegle, L., Jacob, D. J., Heikes, B. G., Snow, J., Kondo, Y., Shetter, R., Sachse, G. W., Anderson, B., Gregory, G. L., Vay, S., Singh, H. B., Davis, D. D., Crawford, J. H., and Blake, D. R.: OH and HO$_2$ chemistry in the North Atlantic free troposphere, Geophys. Res. Lett., 26, 3077–3080, doi:10.1029/1999gl900549, 1999.

Carpenter, L. J., Green, T. J., Mills, G. P., Bauguitte, S., Penkett, S. A., Zanis, P., Schuepbach, E., Schmidbauer, N., Monks, P. S., and Zellweger, C.: Oxidized nitrogen and ozone production efficiencies in the springtime free troposphere over the Alps, J. Geophys. Res.-Atmos., 105, 14547–14559, doi:10.1029/2000jd900002, 2000.

Chemical Kinetics and Photochemical Data for Use in Atmospheric Studies, available at: http://jpldataeval.jpl.nasa.gov (last access: 6 October 2014), 2011.

Chen, G., Davis, D., Crawford, J., Nowak, J. B., Eisele, F., Mauldin, R. L., Tanner, D., Buhr, M., Shetter, R., Lefer, B., Arimoto, R., Hogan, A., and Blake, D.: An investigation of South Pole HO_x chemistry: comparison of model results with ISCAT observations, Geophys. Res. Lett., 28, 3633–3636, doi:10.1029/2001gl013158, 2001.

Davis, D., Nowak, J. B., Chen, G., Buhr, M., Arimoto, R., Hogan, A., Eisele, F., Mauldin, L., Tanner, D., Shetter, R., Lefer, B., and McMurry, P.: Unexpected high levels of NO observed at South Pole, Geophys. Res. Lett., 28, 3625–3628, doi:10.1029/2000gl012584, 2001.

Day, D. A., Wooldridge, P. J., Dillon, M. B., Thornton, J. A., and Cohen, R. C.: A thermal dissociation laser-induced fluorescence instrument for in situ detection of NO_2, peroxy nitrates, alkyl nitrates, and HNO_3, J. Geophys. Res.-Atmos., 107, doi:10.1029/2001jd000779, 2002.

DeMore, W. B., Sander, S. P., Glolden, G. M., Hampson, R. F., Kurylo, M. J., Howeard, C. J., Ravishankara, A. R., Kolb, C. E., and Molina, M. J.: Chemical kinetics and photochemical data for use in stratospheric modeling, Propulsion Laboratory, Pasadena, CA, 1997.

Dusanter, S., Vimal, D., and Stevens, P. S.: Technical note: Measuring tropospheric OH and HO_2 by laser-induced fluorescence at low pressure. A comparison of calibration techniques, Atmos. Chem. Phys., 8, 321–340, doi:10.5194/acp-8-321-2008, 2008.

Edwards, P. M., Brown, S. S., Roberts, J. M., Ahmadov, R., Banta, R. M., deGouw, J. A., Dube, W. P., Field, R. A., Flynn, J. H., Gilman, J. B., Graus, M., Helmig, D., Koss, A., Langford, A. O., Lefer, B. L., Lerner, B. M., Li, R., Li, S. M., McKeen, S. A., Murphy, S. M., Parrish, D. D., Senff, C. J., Soltis, J., Stutz, J., Sweeney, C., Thompson, C. R., Trainer, M. K., Tsai, C., Veres, P. R., Washenfelder, R. A., Warneke, C., Wild, R. J., Young, C. J., Yuan, B., and Zamora, R.: High winter ozone pollution from carbonyl photolysis in an oil and gas basin, Nature, 514, 351–354, doi:10.1038/nature13767, 2014.

Faloona, I., Tan, D., Brune, W. H., Jaegle, L., Jacob, D. J., Kondo, Y., Koike, M., Chatfield, R., Pueschel, R., Ferry, G., Sachse, G., Vay, S., Anderson, B., Hannon, J., and Fuelberg, H.: Observations of HO_x and its relationship with NO_x in the upper troposphere during SONEX, J. Geophys. Res.-Atmos., 105, 3771–3783, doi:10.1029/1999jd900914, 2000.

Febo, A., Perrino, C., Gherardi, M., and Sparapani, R.: Evaluation of a high-purity and high-stability continuous generation system for nitrous acid, Environ. Sci. Technol., 29, 2390–2395, 1995.

Gierczak, T., Jimenez, E., Riffault, V., Burkholder, J. B., and Ravishankara, A. R.: Thermal decomposition of HO_2NO_2 (peroxynitric acid, PNA): rate coefficient and determination of the enthalpy of formation, J. Phys. Chem.-US, 109, 586–596, doi:10.1021/jp046632f, 2005.

Title Page

Abstract | Introduction

Conclusions | References

Tables | Figures

|◄ | ►|

◄ | ►

Back | Close

Full Screen / Esc

Printer-friendly Version

Interactive Discussion

Goldstein, S., Lind, J., and Merenyi, G.: Chemistry of peroxynitrites as compared to peroxynitrates, Chem. Rev., 105, 2457–2470, doi:10.1021/cr0307087, 2005.

Grannas, A. M., Jones, A. E., Dibb, J., Ammann, M., Anastasio, C., Beine, H. J., Bergin, M., Bottenheim, J., Boxe, C. S., Carver, G., Chen, G., Crawford, J. H., Dominé, F., Frey, M. M., Guzmán, M. I., Heard, D. E., Helmig, D., Hoffmann, M. R., Honrath, R. E., Huey, L. G., Hutterli, M., Jacobi, H. W., Klán, P., Lefer, B., McConnell, J., Plane, J., Sander, R., Savarino, J., Shepson, P. B., Simpson, W. R., Sodeau, J. R., von Glasow, R., Weller, R., Wolff, E. W., and Zhu, T.: An overview of snow photochemistry: evidence, mechanisms and impacts, Atmos. Chem. Phys., 7, 4329–4373, doi:10.5194/acp-7-4329-2007, 2007.

Huey, L. G.: Measurement of trace atmospheric species by chemical ionization mass spectrometry: speciation of reactive nitrogen and future directions, Mass Spectrom. Rev., 26, 166–184, doi:10.1002/mas.20118, 2007.

Huey, L. G., Villalta, P. W., Dunlea, E. J., Hanson, D. R., and Howard, C. J.: Reactions of CF_3O^- with atmospheric trace gases, J. Phys. Chem.-US, 100, 190–194, doi:10.1021/jp951928u, 1996.

Huey, L. G., Tanner, D. J., Slusher, D. L., Dibb, J. E., Arimoto, R., Chen, G., Davis, D., Buhr, M. P., Nowak, J. B., Mauldin, R. L., Eisele, F. L., and Kosciuch, E.: CIMS measurements of HNO_3 and SO_2 at the South Pole during ISCAT 2000, Atmos. Environ., 38, 5411–5421, doi:10.1016/j.atmosenv.2004.04.037, 2004.

IUPAC Task Group on Atmosperic Chemical Kinetic Data Evaluation, available at:http://iupac.pole-ether.fr, (last access: December 2014), 2004.

Jimenez, E., Gierczak, T., Stark, H., Burkholder, J. B., and Ravishankara, A. R.: Reaction of OH with HO_2NO_2 (peroxynitric acid): rate coefficients between 218 and 335 K and product yields at 298 K, J. Phys. Chem.-US, 108, 1139–1149, doi:10.1021/jp0363489, 2004.

Jimenez, E., Gierczak, T., Stark, H., Burkholder, J. B., and Ravishankara, A. R.: Quantum yields of OH, HO_2 and NO_3 in the UV photolysis of HO_2NO_2, Phys. Chem. Chem. Phys., 7, 342–348, doi:10.1039/b413429j, 2005.

Jones, A. E., Brough, N., Anderson, P. S., and Wolff, E. W.: HO_2NO_2 and HNO_3 in the coastal Antarctic winter night: a "lab-in-the-field" experiment, Atmos. Chem. Phys., 14, 11843–11851, doi:10.5194/acp-14-11843-2014, 2014.

Keim, C., Liu, G. Y., Blom, C. E., Fischer, H., Gulde, T., Höpfner, M., Piesch, C., Ravegnani, F., Roiger, A., Schlager, H., and Sitnikov, N.: Vertical profile of peroxyacetyl nitrate (PAN) from

Title Page

Abstract | Introduction

Conclusions | References

Tables | Figures

|◄ | ►|

◄ | ►

Back | Close

Full Screen / Esc

Printer-friendly Version

Interactive Discussion

MIPAS-STR measurements over Brazil in February 2005 and its contribution to tropical UT NO_y partitioning, Atmos. Chem. Phys., 8, 4891–4902, doi:10.5194/acp-8-4891-2008, 2008.

Kim, S., Huey, L. G., Stickel, R. E., Tanner, D. J., Crawford, J. H., Olson, J. R., Chen, G., Brune, W. H., Ren, X., Lesher, R., Wooldridge, P. J., Bertram, T. H., Perring, A., Cohen, R. C., Lefer, B. L., Shetter, R. E., Avery, M., Diskin, G., and Sokolik, I.: Measurement of HO_2NO_2 in the free troposphere during the intercontinental chemical transport experiment – North America 2004, J. Geophys. Res.-Atmos., 112, doi:10.1029/2006jd007676, 2007.

Li, Z. J., Friedl, R. R., Moore, S. B., and Sander, S. P.: Interaction of peroxynitric acid with solid H_2O ice, J. Geophys. Res.-Atmos., 101, 6795–6802, doi:10.1029/96jd00065, 1996.

Logager, T. and Sehested, K.: Formation and decay of peroxtnitric acid – a pulse-radiolysis study, J. Phys. Chem.-US, 97, 10047–10052, 1993.

Lyman, S. and Shorthill, H.: Final Report: 2012 Uintah Basin Winter Ozone & Air Quality Study, Utah State University, 281, 2012.

Murphy, J. G., Thornton, J. A., Wooldridge, P. J., Day, D. A., Rosen, R. S., Cantrell, C., Shetter, R. E., Lefer, B., and Cohen, R. C.: Measurements of the sum of HO_2NO_2 and $CH_3O_2NO_2$ in the remote troposphere, Atmos. Chem. Phys., 4, 377–384, doi:10.5194/acp-4-377-2004, 2004.

Niki, H., Maker, P. D., Savage, C. M., and Breitenbach, L. P.: Fourier-Transform IR spectroscopy observation of pernitric acid formed via $HOO + NO_2 \rightarrow HOONO_2$, Chem. Phys. Lett., 45, 564–566, doi:10.1016/0009-2614(77)80090-0, 1977.

Rinsland, C. P., Zander, R., Farmer, C. B., Norton, R. H., Brown, L. R., Russell, J. M., and Park, J. H.: Evidence for the presence of the $802.7\,cm^{-1}$ band Q branch of HO_2NO_2 in high-resolution solar absorption spectra of the stratosphere, Geophys. Res. Lett., 13, 761–764, doi:10.1029/GL013i008p00761, 1986.

Rinsland, C. P., Gunson, M. R., Salawitch, R. J., Michelsen, H. A., Zander, R., Newchurch, M. J., Abbas, M. M., Abrams, M. C., Manney, G. L., Chang, A. Y., Irion, F. W., Goldman, A., and Mahieu, E.: ATMOS/ATLAS-3 measurements of stratospheric chlorine and reactive nitrogen partitioning inside and outside the November 1994 Antarctic vortex, Geophys. Res. Lett., 23, 2365–2368, doi:10.1029/96gl01474, 1996.

Roberts, J. M., Veres, P., Warneke, C., Neuman, J. A., Washenfelder, R. A., Brown, S. S., Baasandorj, M., Burkholder, J. B., Burling, I. R., Johnson, T. J., Yokelson, R. J., and de Gouw, J.: Measurement of HONO, HNCO, and other inorganic acids by negative-ion

Title Page

Abstract | Introduction

Conclusions | References

Tables | Figures

|◄ | ►|

◄ | ►

Back | Close

Full Screen / Esc

Printer-friendly Version

Interactive Discussion

proton-transfer chemical-ionization mass spectrometry (NI-PT-CIMS): application to biomass burning emissions, Atmos. Meas. Tech., 3, 981–990, doi:10.5194/amt-3-981-2010, 2010.

Roehl, C. M., Nizkorodov, S. A., Zhang, H., Blake, G. A., and Wennberg, P. O.: Photodissociation of peroxynitric acid in the near-IR, J. Phys. Chem.-US, 106, 3766–3772, doi:10.1021/jp013536v, 2002.

Salawitch, R. J., Wennberg, P. O., Toon, G. C., Sen, B., and Blavier, J. F.: Near IR photolysis of HO_2NO_2: implications for HO_x, Geophys. Res. Lett., 29, doi:10.1029/2002gl015006, 2002.

Sen, B., Toon, G. C., Osterman, G. B., Blavier, J. F., Margitan, J. J., Salawitch, R. J., and Yue, G. K.: Measurements of reactive nitrogen in the stratosphere, J. Geophys. Res.-Atmos., 103, 3571–3585, doi:10.1029/97jd02468, 1998.

Singh, H. B., Brune, W. H., Crawford, J. H., Jacob, D. J., and Russell, P. B.: Overview of the summer 2004 intercontinental chemical transport experiment – North America (INTEX-A), J. Geophys. Res.-Atmos., 111, doi:10.1029/2006jd007905, 2006.

Singh, H. B., Salas, L., Herlth, D., Kolyer, R., Czech, E., Avery, M., Crawford, J. H., Pierce, R. B., Sachse, G. W., Blake, D. R., Cohen, R. C., Bertram, T. H., Perring, A., Wooldridge, P. J., Dibb, J., Huey, G., Hudman, R. C., Turquety, S., Emmons, L. K., Flocke, F., Tang, Y., Carmichael, G. R., and Horowitz, L. W.: Reactive nitrogen distribution and partitioning in the North American troposphere and lowermost stratosphere, J. Geophys. Res.-Atmos., 112, doi:10.1029/2006jd007664, 2007.

Slusher, D. L., Pitteri, S. J., Haman, B. J., Tanner, D. J., and Huey, L. G.: A chemical ionization technique for measurement of pernitric acid in the upper troposphere and the polar boundary layer, Geophys. Res. Lett., 28, 3875–3878, doi:10.1029/2001gl013443, 2001.

Slusher, D. L., Huey, L. G., Tanner, D. J., Chen, G., Davis, D. D., Buhr, M., Nowak, J. B., Eisele, F. L., Kosciuch, E., Mauldin, R. L., Lefer, B. L., Shetter, R. E., and Dibb, J. E.: Measurements of pernitric acid at the South Pole during ISCAT 2000, Geophys. Res. Lett., 29, doi:10.1029/2002gl015703, 2002.

Slusher, D. L., Huey, L. G., Tanner, D. J., Flocke, F. M., and Roberts, J. M.: A thermal dissociation-chemical ionization mass spectrometry (TD-CIMS) technique for the simultaneous measurement of peroxyacyl nitrates and dintrogen pentoxide, J. Geophys. Res.-Atmos., 109, D19315, doi:10.1029/2004JD004670, 2004.

Slusher, D. L., Neff, W. D., Kim, S., Huey, L. G., Wang, Y., Zeng, T., Tanner, D. J., Blake, D. R., Beyersdorf, A., Lefer, B. L., Crawford, J. H., Eisele, F. L., Mauldin, R. L., Kosciuch, E., Buhr, M. P., Wallace, H. W., and Davis, D. D.: Atmospheric chemistry re-

sults from the ANTCI 2005 Antarctic plateau airborne study, J. Geophys. Res.-Atmos., 115, doi:10.1029/2009jd012605, 2010.

Spencer, K. M., McCabe, D. C., Crounse, J. D., Olson, J. R., Crawford, J. H., Weinheimer, A. J., Knapp, D. J., Montzka, D. D., Cantrell, C. A., Hornbrook, R. S., Mauldin III, R. L., and Wennberg, P. O.: Inferring ozone production in an urban atmosphere using measurements of peroxynitric acid, Atmos. Chem. Phys., 9, 3697–3707, doi:10.5194/acp-9-3697-2009, 2009.

Stark, H., Brown, S. S., Burkholder, J. B., Aldener, M., Riffault, V., Gierczak, T., and Ravishankara, A. R.: Overtone dissociation of peroxynitric acid (HO_2NO_2): absorption cross sections and photolysis products, J. Phys. Chem.-US, 112, 9296–9303, doi:10.1021/jp802259z, 2008.

Uinta Basin Winter Ozone Study Final Report 2013, available at: http://rd.usu.edu/files/uploads/2013_final_report_ubos.pdf (last access: July), 2014.

Ulrich, T., Ammann, M., Leutwyler, S., and Bartels-Rausch, T.: The adsorption of peroxynitric acid on ice between 230 K and 253 K, Atmos. Chem. Phys., 12, 1833–1845, doi:10.5194/acp-12-1833-2012, 2012.

VandenBoer, T. C., Young, C. J., Talukdar, R. K., Markovic, M. Z., Brown, S. S., Roberts, J. M., and Murphy, J. G.: Nocturnal loss and daytime source of nitrous acid through reactive uptake and displacement, Nat. Geosci., 8, 55–60, doi:10.1038/ngeo2298, 2015.

Wang, X., Wang, T., Yan, C., Tham, Y. J., Xue, L., Xu, Z., and Zha, Q.: Large daytime signals of N_2O_5 and NO_3 inferred at 62 amu in a TD-CIMS: chemical interference or a real atmospheric phenomenon?, Atmos. Meas. Tech., 7, 1–12, doi:10.5194/amt-7-1-2014, 2014.

Wennberg, P. O., Salawitch, R. J., Donaldson, D. J., Hanisco, T. F., Lanzendorf, E. J., Perkins, K. K., Lloyd, S. A., Vaida, V., Gao, R. S., Hintsa, E. J., Cohen, R. C., Swartz, W. H., Kusterer, T. L., and Anderson, D. E.: Twilight observations suggest unknown sources of HO_x, Geophys. Res. Lett., 26, 1373–1376, doi:10.1029/1999gl900255, 1999.

Wild, R., Edwards, P., Dube, W. P., Baumann, K., Edgerton, E. S., Quinn, P. Q., Roberts, J. M., Rollins, A. W., Veres, P. R., Warneke, C., Williams, E. J., Yuan, B., and Brown, S.: A measurement of total reactive nitrogen, NO_y, together with NO_2, NO, and O_3 via cavity ring-down spectroscopy, Environ. Sci. Tech., 48, 9609–9615, doi:10.1021/es501896w, 2014.

Williams, J., Roberts, J. M., Bertman, S. B., Stroud, C. A., Fehsenfeld, F. C., Baumann, K., Buhr, M. P., Knapp, K., Murphy, P. C., Nowick, M., and Williams, E. J.: A method for the airborne measurement of PAN, PPN, and MPAN, J. Geophys. Res.-Atmos., 105, 28943–28960, 2000.

Wooldridge, P. J., Perring, A. E., Bertram, T. H., Flocke, F. M., Roberts, J. M., Singh, H. B., Huey, L. G., Thornton, J. A., Wolfe, G. M., Murphy, J. G., Fry, J. L., Rollins, A. W., LaFranchi, B. W., and Cohen, R. C.: Total Peroxy Nitrates (ΣPNs) in the atmosphere: the Thermal Dissociation-Laser Induced Fluorescence (TD-LIF) technique and comparisons to speciated PAN measurements, Atmos. Meas. Tech., 3, 593–607, doi:10.5194/amt-3-593-2010, 2010.

Zhang, R. Y., Leu, M. T., and Keyser, L. F.: Heterogeneous chemistry of HO_2NO_2 in liquid sulfuric acid, J. Phys. Chem.-US, 101, 3324–3330, doi:10.1021/jp963321z, 1997.

Zhu, T., Yarwood, G., Chen, J., and Niki, H.: Evidence for the heterogeneous formation of nitrous acid from peroxynitric acid in environmental chambers, Environ. Sci. Technol., 27, 982–983, doi:10.1021/es00042a024, 1993.

Table 1. Summary of observed products, sensitivities, and detection limits (DL) for the reaction of I$^-$ with HO$_2$NO$_2$, HONO and HO$_2$.

Analyte	Detected Ion (m/z)	Sensitivity[a] (Hz pptv^{-1})	DL (pptv, 3σ)	Inlet[a]
HO$_2$NO$_2$	I-HO$_2$NO$_2^-$ (206)	0.40 ± 0.06	20	Cold
	NO$_3^-$ (62)	144 ± 11[b]	0.7	Cold, Hot
	I-HO$_2^-$ (160)	2.0 ± 0.04	40	Hot
HONO	I-HONO$^-$ (174)	1.7 ± 0.3	30	Cold, Hot
HO$_2$	I-HO$_2^-$ (160)	2.6 ± 0.3	20	Cold, Hot

[a] Indicates the inlet dissociation temperature at which the particular ion can be sensitively observed. The inlet dissociator was operated at a temperature of 130 ˚C (Hot) or at ambient temperature (Cold).
[b] Sensitivity reported is for detection with an inlet dissociator at ambient temperature (Cold).
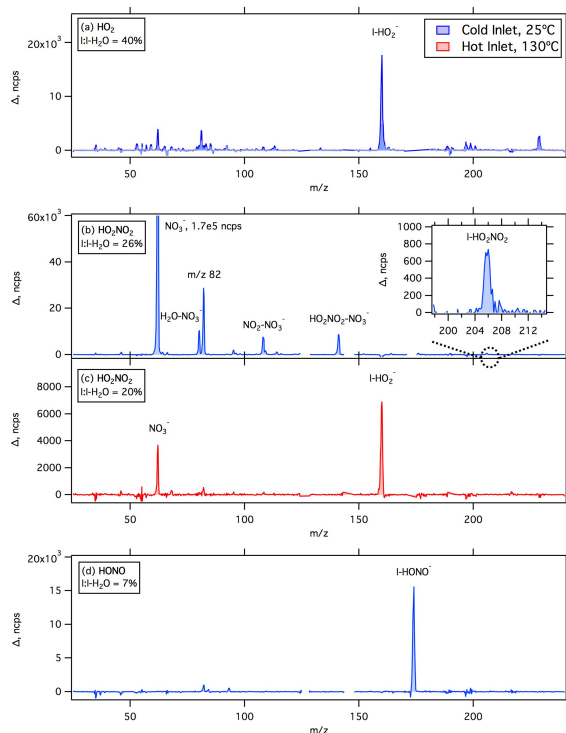
Figure 1. Shown are normalized (10^6 cps I$^-$), background corrected mass spectra acquired in the laboratory for calibration sources of HO$_2$ **(a)**, HO$_2$NO$_2$ **(b)** and **(c)**, and HONO **(d)**. Spectra colored in blue were collected using a room temperature inlet ($\sim 25\,°C$) while spectra in red indicate that an inlet dissociator at a temperature of $130\,°C$ was used. Background mass spectra have been subtracted from the displayed mass spectra to highlight the m/z ions that are produced via the I$^-$ CIMS ion chemistry. The graph inset in Fig. 1b shows a magnified view of the region in the dashed circle where the parent ion cluster (I-HO$_2$NO$_2^-$) is detected. All three species are detectable at a unique m/z, when an inlet dissociator is not used, allowing for simultaneous detection of HO$_2$, HO$_2$NO$_2$, and HONO.
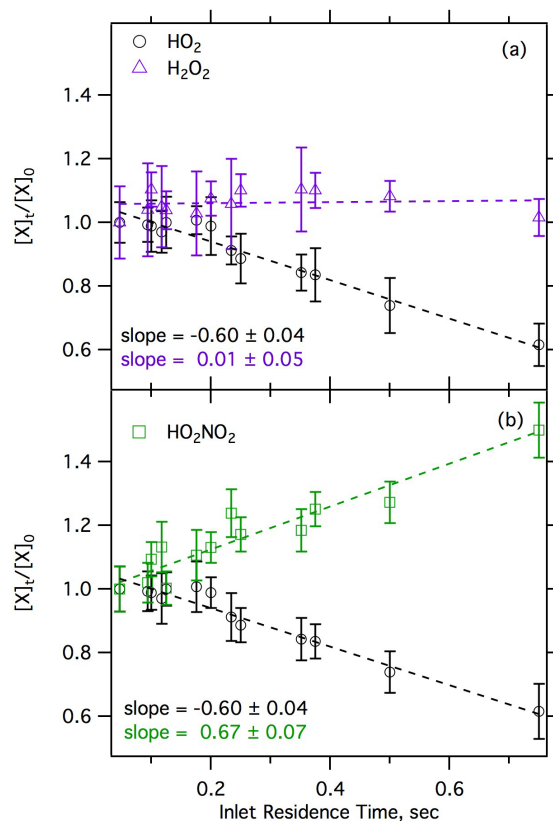
Figure 2. Observed losses vs. inlet residence times for a generated standard of HO_2 radicals sampled through PFA tubing at various flow rates (3–6 slpm) and lengths (0–3 m). Concentrations have been normalized to the initial concentration observed at the minimum reaction time displayed. Reaction with NO_2 to form HO_2NO_2 appears to be the dominant loss for HO_2 on these timescales.
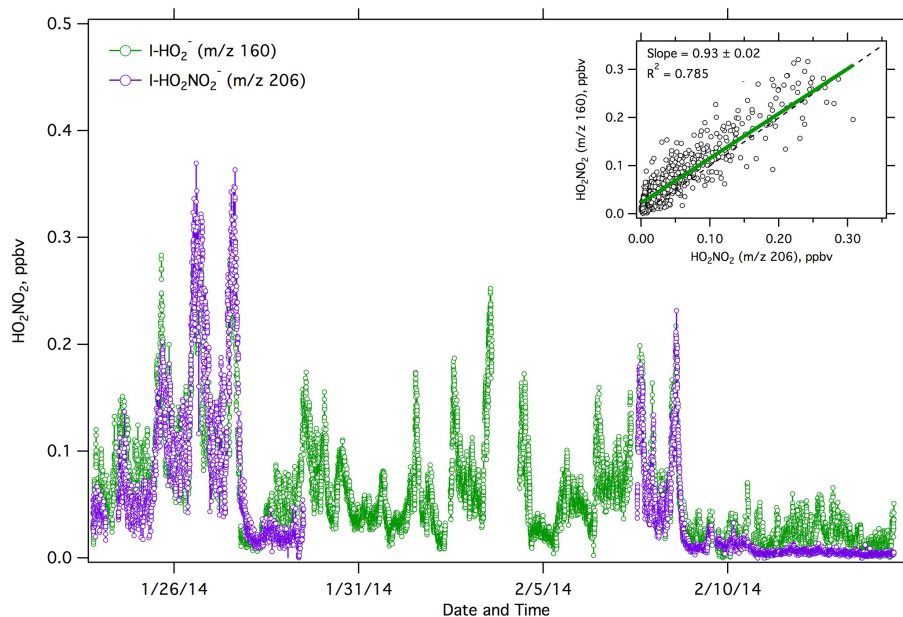
Figure 3. A comparison of HO_2NO_2 observations made using the $I\text{-}HO_2^-$ (m/z 160) ion with a hot dissociator (130 °C) and the $I\text{-}HO_2NO_2^-$ (m/z 206) ion with a cold dissociator ($\sim$ 25 °C). Inset is a correlation plot of the two measurements where comparison is possible.
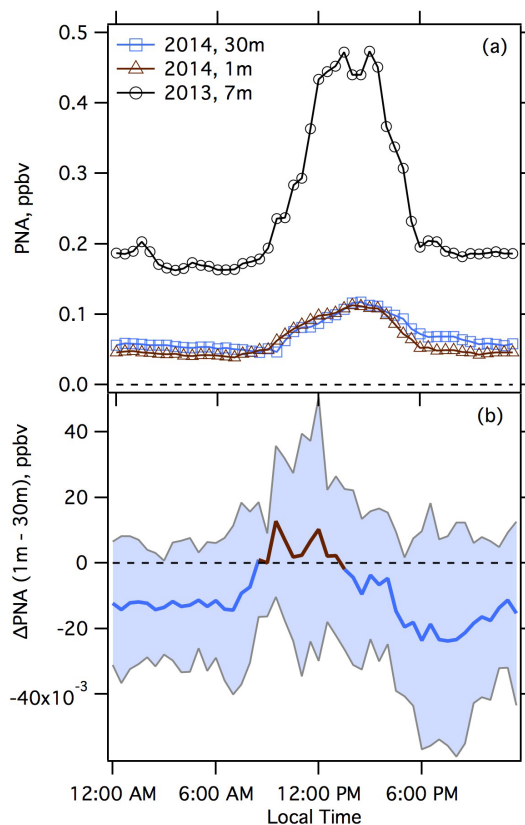
Figure 4. Diurnal profiles of PNA are shown in **(a)** for the full measurement period during the UBWOS 2013 and 2014 studies, with the 2013 study separated based on the sampling height location. The difference of the 2013 study 1 and 30 m PNA measurement, where a positive value (brown) indicates larger concentrations at the ground and a negative value (blue) suggests a relative PNA depletion in the 1 m measurement.
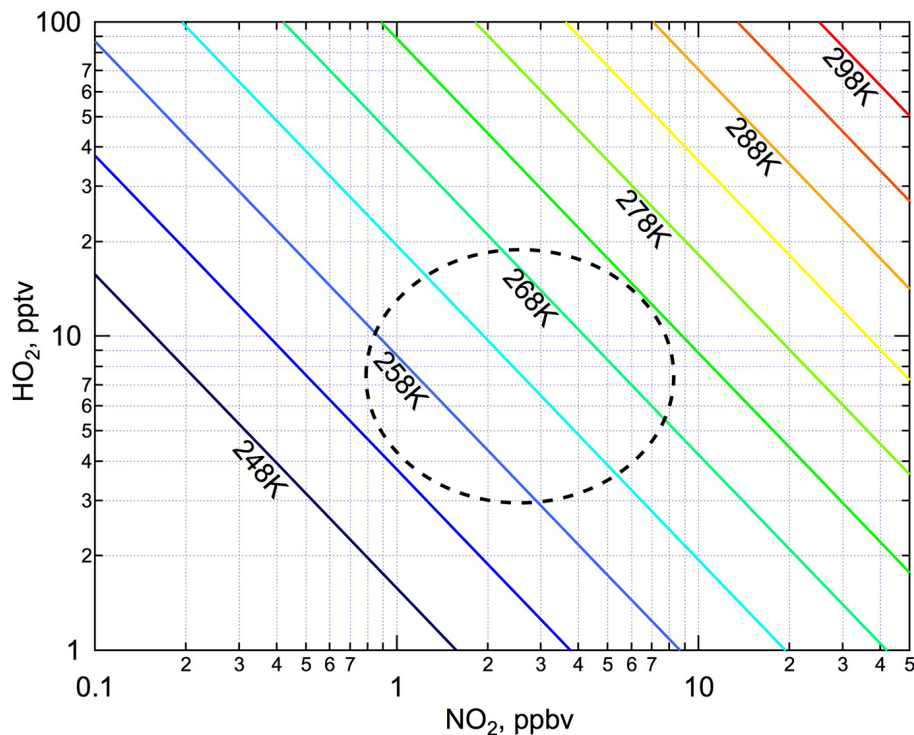
Figure 5. Temperature and mixing ratios of HO_2 and NO_2 required to sustain an equilibrium concentration of $1\,ppbv\,HO_2NO_2$. The region within the dashed circle superimposed on the figure highlights the conditions encountered during the 2013 UBWOS study. Data shown was calculated using the IUPAC database (Atkinson et al., 2004).
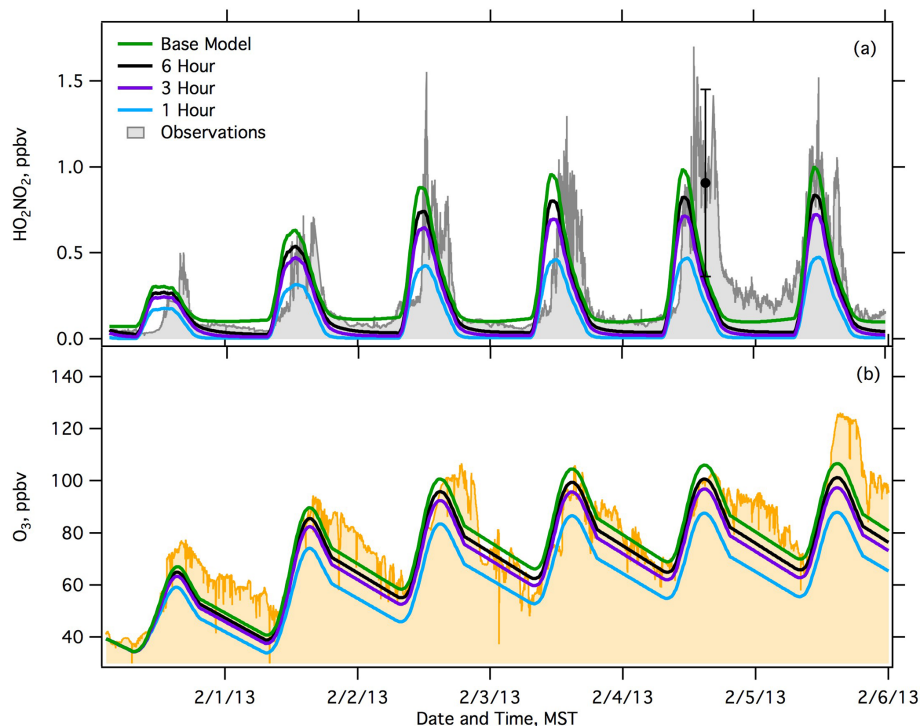
Figure 6. Comparison of PNA and ozone observations throughout an ozone formation event observed during UBWOS 2013 and corresponding model predictions using an explicit chemical box model describing the chemistry. **(a)** HO_2NO_2 observations compared to model results applying various PNA lifetimes with respect to deposition (t_{PNA}). The datum shown with error bars, black circle, represents the approximated 60 % error on the 2013 HO_2NO_2 I^- CIMS measurements. **(b)** illustrates the effect varying deposition rates of PNA has on total predicted ozone production.

Title Page

Abstract | Introduction

Conclusions | References

Tables | Figures

|◄ | ►|

◄ | ►

Back | Close

Full Screen / Esc
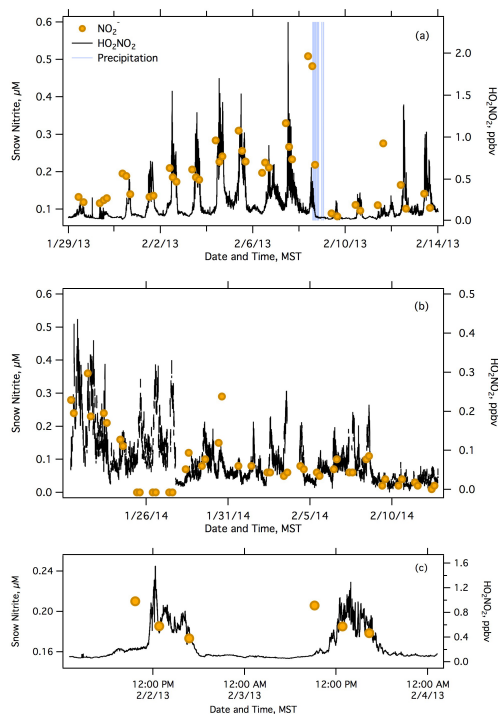
Printer-friendly Version

Interactive Discussion

Figure 7. Displayed are gas phase HO_2NO_2 observations made during two wintertime ozone events in the Uintah Basin, UT observed in 2013 **(a)**, and through the entire 2014 study **(b)**. Measurements of the nitrite content of the snow surface taken during the same time periods are also shown. In 2013, a precipitation event that occurred on the afternoon of 8 February, shown as the period in blue, added fresh surface snow and flushed pollutants out of the basin resulting in lower ambient PNA and snow nitrite levels. **(c)** shows in more detail a period from the 2013 measurements to better illustrate the daily reduction in snow surface nitrate that was regularly observed.